Compressed Sensing MRI With Phase Noise Disturbance Based on Adaptive Tight Frame and Total Variation

FAN XIAOYU[1,2], LIAN QIUSHENG[1], AND SHI BAOSHUN[1,3]

[1]School of Information Science and Engineering, Yanshan University, Qinhuangdao 066004, China
[2]School of Electrical and Electronic Engineering, Anhui Science and Technology University, Chuzhou 233100, China
[3]CETC Key Laboratory of Aerospace Information Applications, Shijiazhuang 050081, China

Corresponding author: Lian Qiusheng (lianqs@ysu.edu.cn)

ABSTRACT Magnetic resonance imaging (MRI) has been widely employed in medical diagnosis, since it enables superior visualization of anatomical structure with noninvasive and nonionizing radiation nature. However, during the data acquisition process of MRI, patients' translational motion usually leads to phase changes of the observed data; moreover, the amplitudes of the observed data are usually contaminated by noises. In this paper, we assume that the phase and amplitude noises, respectively, cause the phase and amplitude changes of the observed data. Therefore, how to reconstruct high-quality magnetic resonance (MR) images via highly undersampled K-space data with noises is a challenge. To address this issue, a novel MR image reconstruction model, named the adaptive tight frame and total variation MR image reconstruction model (TFTV-MRI), is proposed based on the compressed sensing (CS) theory. TFTV-MRI fuses the adaptive tight frame (ATF) learning and total variation (TV) into the image reconstruction model. The sparse representations of MR images in tight frame domain can adapt to the MR image by itself, simultaneously, the advantage of TV is better edge preserving property and MR images are sparse in gradient domain. Differing from the l_0-norm or l_1-norm utilized in traditional AFT learning, we exploit the logarithm penalty term to measure the sparsity of MR images in TFTV-MRI. The alternating iterative minimization algorithm is utilized to tackle the optimization problem of TFTV-MRI, including ATF learning step and MR image reconstruction step. In MR image reconstruction step, the inertial proximal algorithm for nonconvex optimization is employed. The experiments verified that the proposed model achieved the superior performance for dislodging the phase noises caused by the translational motion and removing the amplitude noises of the observed data, and reconstructed MR images nicely in different sampling schemes. Compared with the existing methods, the proposed approach can achieve higher accurate image reconstruction quality, faster convergence speed, and better robustness to noises.

INDEX TERMS MRI, image reconstruction, sparse representation, adaptive tight frame, TV regularization.

I. INTRODUCTION

With the rapid development of medical image processing technology, MRI has been widely used in medical clinical examination, becoming an important means of medical diagnosis [1]. However, in practical medical applications, high-quality MR images obtained by conventional methods require large amounts of sampling data. The process of acquiring data needs more time during which the patient is susceptible to have slight translational motion (especially for children, stroke, and Parkinson patients) or the organ itself may have motion (such as pulse), which will lead to motion artifacts owing to phase changes of the sampling data [2]–[4]. The phase changes are regarded as phases of the sampling data disturbed by noises (called phase noises) in this paper. Meanwhile, the longer the data acquisition time is, the greater the probability of the system to produce noises will be. It will lead to amplitudes of the sampling data contaminated by noises (called amplitude noises in this paper). Phase and

amplitude noises make the MR image blurred and limit the MR image for medical applications, which has become a key factor to restrict the further improvement of MR imaging quality at present. Therefore, how to establish an excellent reconstruction model which can achieve MR images with high-quality reconstruction form highly undersampled K-space data is a challenge.

The problems of amplitude noise removal and phase correction of motion artifacts in MR images have been an active research field. The main methods to solve these problems are to acquire more K-space data, to use the special sampling sequence for acquiring samples, and to exploit the advanced algorithm for carrying on the post-processing of the image. Researchers have proposed lots of algorithms to suppress amplitude and phase noises in succession. The early algorithm is to assume that the region of interest (ROI) is a prior known [2], [3], and to correct phase of motion artifacts employing the idea of phase retrieval [4]. This algorithm contributes to phase correction when oversampling the frequency domain of the image in a relatively small ROI. Subsequently, navigator-based echo technique (NBET) [5], [6] is developed for phase correction of motion artifacts. This technique can detect motion phases between the ''navigator'' and a reference point without phase change, and then resolve an ill-posed problem by acquiring extra ''navigator''. In [7], the phase denoising of motion artifacts for MR images is attained by the genetic algorithm, and the translational phase noises of motion artifacts are dislodged in global optimization of the translational motion. In [8], the phase of the MR image is estimated by exploiting the correlations between a small number of adjacent readout lines of the motion. This method requires data oversampling in the phase encoding direction in order to satisfy existences of the correlations between adjacent readout lines. In [9], an improved region growing algorithm is proposed for phase denoising of Dixon water and fat MR images. In this algorithm, a spatial angular continuity vector is selected from the two candidate vectors of each pixel, and the direction of the output vector map is spatially smooth. However, the algorithm requires that the phase differences of two candidate vectors for each pixel must be known or can be calculated.

In 2006, the CS theory [10], [11] proposed by Donoho and Candes et al. showed that the original signal can be reconstructed from a few examples of undersampled data based on the assumption that the signal is compressible or sparse in a certain transform domain. Since medical MR images are sparse in some transform domain, the CS has been widely developed in many biomedical imaging systems [12]–[14], such as CT imaging, ultrasound medical imaging and so on. At present, CS has been applied to MR rapid imaging [15], [16]. CS-based MR imaging can reconstruct high-quality images with highly undersampled data in K-space, shorten MRI scan time significantly for patients, and speed up the image processing. Therefore, how to reconstruct MR images from highly undersampled K-space data employing the sparse regularizations is of great interest

to researchers. Lusting et al. first applied the CS theory to MR image reconstruction, in which the problem of undersampled image reconstruction was expressed as an l_1-norm minimization problem [17]. In order to improve the speed and precision of image reconstruction, TV regularization is proposed to the reconstruction model to enhance the sparsity of the MR image for ensuring high-quality image reconstruction. Barral et al. proposed a phase denoising method for motion artifacts based on the fusion of CS and NBET [18]. This method is only used for phase denoising in the condition that the phase can turn back to the original position after motion. As it is difficult for the object to return to the initial position after motion, so the method has limitations in practical application. In the above algorithms, sparse approximations of MR images are nonadaptive; the transform or dictionary is designed in advance, whose adaptability to MR image is usually not optimal. Hence, these algorithms are generally limited for MR image reconstruction when undersampled measurements get much fewer [19]. For the sake of enhancing the self-adaptability of the dictionary, the dictionary learning algorithm is exploited for the MR image reconstruction. Saiprasad et al. proposed an adaptive synthesis dictionary learning framework (DLMRI) based on the K-SVD algorithm [19]. DLMRI is an MR image reconstruction framework combining CS with synthesis dictionary learning, and DLMRI can achieve significantly superior image reconstructions. However, DLMRI involves synthesis sparse coding step that is computationally expensive. In [20], transform learning MR image reconstruction model (TLMRI) is proposed for simultaneously adaptive sparsifying transform learning and image reconstruction, which achieves better reconstruction quality and much faster reconstruction speed than those of DLMRI. In [21], the phase denoising of motion artifacts is performed by employing the sparsity of the l_1-norm regularization. Assume that the K-space data of the image have a little motion on a single readout line, and the method regards the little motion as an unknown system parameter, then the unknown system parameter is estimated by employing the redundant information of all K-space sampled data, and combining with image reconstruction process. In [22], the data-driven tight frame magnetic image reconstruction (DDTF-MRI) method is proposed to reconstruct the undersampled MR image by using the adaptive tight frame learning with the l_1-norm regularization. The DDTF-MRI further improves the image reconstruction accuracy and reduces the complexity of the algorithm. In [23], another phase denoising method of motion artifacts is proposed with navigator echo combined with CS. This method fuses the conventional gradient echo sequence with the navigator echo technique, is employed to monitor the motion information, and acquires the data by a specific phase encoding sequence. Then, the MR image is reconstructed with the unaffected data by the CS method.

All the above algorithms have made some progresses in removing the phase noises of motion artifacts or MR image amplitude noises. However, how to further improve the

MR image reconstruction quality from more highly under-sampled measurements by exploiting more prior knowledge of the image is still a crucial issue. To address this issue, MR images are reconstructed from highly undersampled K-space data of CS based on the sparsity of images in ATF and gradient domain in this paper. Compared with the traditional algorithms, ATF learning method can achieve better sparse representations of images, more nicely image reconstruction quality, and faster image reconstruction speed with much fewer sampling data. Simultaneously, TV with gradient preserving property can be applied to the image reconstruction model. Hence, MR images can be accurately reconstructed from the highly undersampled measurements by utilizing ATF learning and TV regularization together so as to eliminate phase and amplitude noises of images in this paper.

The rest of this paper is organized as follows: Section II presents the preliminary and prior work in TV regularization and ATF learning for MR images; Section III elaborates our proposed problem formulation of the MR image reconstruction based on ATF learning and TV; Section IV demonstrates the proposed model has the ability for improving MR image reconstruction quality by employing different sampling schemes and noise levels; and Section V concludes with topics and future works are given for the end.

II. BACKGROUND

In this section, we introduce some CS theoretical models for MR image reconstruction. The following notational conventions are utilized throughout the full text. Let $x \in R^N$ represent an underlying MR image, $F_u \in R^{M \times N}$ denote an undersampled Fourier coding matrix, $y \in R^M$ represent undersampled K-space measurements, and $\lambda > 0$ is a penalty parameter.

One of the key problems for CS theory is the choice of sparsiting regularization which can make the underlying image have a perfectly sparse approximation under a certain system. In general, the sparse approximation can be implemented in several ways, which may be a transform, a frame or a general dictionary, such as sparsifying transform, wavelet tight frame. In this paper, TV-based sparse representation and adaptive tight frame learning are studied.

A. TV REGULARIZATION

The sparse representation in gradient domain is a commonly form of the MR image sparse representations, in which the gradient sparsity of the image is regarded as prior knowledge. If the MR image satisfies the gradient sparsity, the desired image x is reconstructed from the undersampled measurements y by the following formulation [17]:

$$\min_{x} \frac{1}{2} \|F_u x - y\|_2^2 + \lambda \|x\|_{\text{TV}}, \qquad (1)$$

where $\|x\|_{\text{TV}} = \|\nabla x\|_1$ denotes the anisotropic formulation of TV semi-norm, and $\nabla = [\nabla_1, \nabla_2]$ represents the difference operators in the horizontal and vertical directions. The term $\|F_u x - y\|_2^2$ is a data fidelity in K-space. The model has much

better ability to preserve the edge property of the MR image. However, many MR images are not obvious piecewise constant, so the model in Eq. (1) is limited in practical application. In [24], RecPF was proposed, in which the fast variable splitting and alternating direction methods were employed to tackle the following unconstrained optimization model as Eq. (2):

$$\min_{x} \frac{1}{2} \|F_u x - y\|_2^2 + \lambda_1 \|x\|_{\text{TV}} + \lambda_2 \|\psi x\|_1. \qquad (2)$$

Here, ψ is a wavelet transform; λ_1 and λ_2 are positive parameters for adjusting data fidelity term and the regularization terms. Eq. (2) is gained by adding a wavelet transform regularization term in Eq. (1) in order to improve the drawback of Eq. (1), and promote the reconstruction quality of MR images. In [25], the gradients of MR images are reconstructed by synthesis dictionary learning, and the model learns gradient dictionaries in gradient domain. The gradients with the dictionary learning are much sparser than the gradients of the image itself for sparse representation. The cost function of the model is Eq. (3) as follows:

$$\min_{x, D^{(i)}, \Gamma^{(i)}} \sum_{i=1}^{2} \sum_{l} \left\| D^{(i)} \alpha_l^{(i)} - R_l(\nabla_{(i)} x) \right\|_2^2 + \frac{\lambda}{2} \|F_u x - y\|_2^2$$
$$s.t. \left\| \alpha_l^{(i)} \right\|_0 \le T_0, \quad \forall l, i, \qquad (3)$$

where $R_l(\cdot)$ indicates the operator that extracts the lth gradient patch from the MR image, and α_l is the synthesis sparse coefficient for the lth gradient patch of the image with sparsity T_0. In Eq. (3), the term $\sum_{i=1}^{2} \sum_{l} \left\| D^{(i)} \alpha_l^{(i)} - R_l(\nabla_{(i)} x) \right\|_2^2$ can capture the sparse prior of gradient image patches by synthesis dictionary learning [25]. This model has the superiority in terms of reconstruction accuracy and convergence for the MR image reconstruction. However, this model also has a drawback which is computationally expensive when synthesis sparse coefficients are solved by using orthogonal matching pursuit method.

B. ADAPTIVE TIGHT FRAME LEARNING

A tight frame is a kind of sparsity-based regularizations, and can be employed for a sparse representation of an image. Due to flexible properties of the tight frame, it has been widely applied in the image processing filed, such as MR image reconstruction by ATF learning [22], natural image denoising and so on. More recently, data-driven tight frame (DDTF) has attracted more attention because of its prominent capabilities, such as adaptive for the image, better sparse approximation to the image, and faster computationally speed under the support of CS.

In [26], DDTF-based construction method was proposed, and was developed for natural image denoising. DDTF with low computation cost performs better than wavelet tight frames in image denoising. The optimization model for constructing DDTF directly from the input image is the following

minimization problem [26]:

$$\min_{\boldsymbol{W}, \boldsymbol{v}} \|\boldsymbol{v} - \boldsymbol{W}\boldsymbol{x}\|_2^2 + \lambda \|\boldsymbol{v}\|_0 \quad s.t. \ \boldsymbol{W}^T\boldsymbol{W} = \boldsymbol{I}. \tag{4}$$

Here, $\boldsymbol{W}$ is an adaptive tight frame, which can be generated by the filter bank; $\boldsymbol{v}$ is a sparse coefficient vector for attaining DDTF. The term $\|\boldsymbol{v} - \boldsymbol{W}\boldsymbol{x}\|_2^2$ in Eq. (4) is used to ensure that the sparse coefficient vector $\boldsymbol{v}$ is close to the canonical coefficient vector of the image $\boldsymbol{x}$ under the analysis of $\boldsymbol{W}$; the term $\|\boldsymbol{v}\|_0$ is used to guarantee the sparsity of $\boldsymbol{v}$; the constraint term $\boldsymbol{W}^T\boldsymbol{W} = \boldsymbol{I}$ is to make sure that $\boldsymbol{W}$ is a tight frame. In [26], $\boldsymbol{v}$ and $\boldsymbol{W}$ of Eq. (4) are respectively solved with alternating iterative minimization method. The alternating minimization involves a solving $\boldsymbol{v}$ step and an updating $\boldsymbol{W}$ step. In the solving $\boldsymbol{v}$ step, Eq. (4) is tackled with fixed $\boldsymbol{W}$ as

$$\min_{\boldsymbol{v}} \|\boldsymbol{v} - \boldsymbol{W}\boldsymbol{x}\|_2^2 + \lambda \|\boldsymbol{v}\|_0. \tag{5}$$

The solution to Eq. (5) can be acquired exactly by the hard threshold method. In the updating $\boldsymbol{W}$ step, Eq. (4) is expressed with fixed $\boldsymbol{v}$ as

$$\min_{\boldsymbol{W}} \|\boldsymbol{v} - \boldsymbol{W}\boldsymbol{x}\|_2^2 \quad s.t. \ \boldsymbol{W}^T\boldsymbol{W} = \boldsymbol{I}. \tag{6}$$

The solution to Eq. (6) can be found using the singular value decomposition (SVD) method in virtue of the filter bank [26].

Recently, ATF has been employed for the MR image reconstruction owing to its significant advantages. A DDTF-based MR image reconstruction model (DDTF-MRI) is proposed in [22]. The model is devoted to effectively enhance sparsity using DDTF learning in the form of l_1-norm under the frame domain, and then reconstructs the MR image. The objective function of the DDTF-MRI model is

$$\min_{\boldsymbol{x}, \boldsymbol{W}} \|\boldsymbol{W}\boldsymbol{x}\|_1 \quad s.t. \ \|\boldsymbol{y} - \boldsymbol{F}_u\boldsymbol{x}\|_2^2 \le \sigma^2, \quad \boldsymbol{W}^T\boldsymbol{W} = \boldsymbol{I}. \tag{7}$$

Where, σ is the noise standard deviation. In [22], the two-level Bregman iterative algorithm is developed to solve Eq. (7), and encouraging performances in MR image reconstruction are achieved. Other fast approaches, such as the orthogonal and multiclass dictionary learning [27] also can construct a tight frame for sparse MRI, and the approaches can further improve the image reconstruction quality.

III. THE PROPOSED TFTV-MRI MODEL
A. PROBLEM FORMULATION
In order to further improve the reconstruction quality of the MR image, this paper focuses on exploiting more sparse priors. In CS theory, gradients of an MR image are sparse using TV regularization that has some desirable properties such as simplicity, convexity, and ability to preserve edges; ATF learning can obtain the ATF that is a sparse representation scheme of the image in transform domain, and the sparsity of an MR image can be scaled by the ATF. In this paper, a novel TFTV-MRI model which fuses the logarithm norm [28] ATF (LATF) learning and TV regularization is proposed. The double sparse TFTV-MRI is applied to

MR image reconstruction with phase and amplitude noises based on making good use of the two sparse priors. The proposed TFTV-MRI model can be described as

$$\min_{\boldsymbol{W}, \boldsymbol{x}} \sum_i \ln(1 + (\boldsymbol{W}\boldsymbol{x})_i^2) + \eta \mathrm{TV}(\boldsymbol{x})$$
$$s.t. \ \boldsymbol{W}^T\boldsymbol{W} = \boldsymbol{I}, \quad \boldsymbol{x} \in C, \ \forall i, \tag{8}$$

where $C = \{\boldsymbol{x} \,|\, |\,|\boldsymbol{y}| - |\boldsymbol{F}_u\boldsymbol{x}|\,| \le \varepsilon, |\angle\boldsymbol{y} - \angle\boldsymbol{F}_u\boldsymbol{x}| \le \delta\}$.

Define $\|\boldsymbol{W}\boldsymbol{x}\|_{\log} = \sum_i \ln(1 + (\boldsymbol{W}\boldsymbol{x})_i^2)$ as the logarithm norm [28] in this paper. The logarithm operation is simple, derivable and calculable; the LATF can measure the sparsity of MR images in transform domain, and capture features of MR images effectively. According to the definition of the logarithm norm, Eq. (8) can be expressed as following:

$$\min_{\boldsymbol{W}, \boldsymbol{x}} \ \|\boldsymbol{W}\boldsymbol{x}\|_{\log} + \eta \mathrm{TV}(\boldsymbol{x}) \quad s.t. \ \boldsymbol{W}^T\boldsymbol{W} = \boldsymbol{I}, \quad \boldsymbol{x} \in C, \ \forall i. \tag{9}$$

In Eq. (9), the term $\|\boldsymbol{W}\boldsymbol{x}\|_{\log}$ denotes the LATF sparsity regularization for the MR image $\boldsymbol{x}$, which can make sure that $\boldsymbol{x}$ is sparse under the analysis of $\boldsymbol{W}$, and the term can be used to learn $\boldsymbol{W}$. The term $\mathrm{TV}(\boldsymbol{x})$ denotes the isotropic discretization formulation of the total variation for $\boldsymbol{x}$, and its formula is $\mathrm{TV}(\boldsymbol{x}) = \sum_i \sqrt{(\boldsymbol{D}_1\boldsymbol{x})_i^2 + (\boldsymbol{D}_2\boldsymbol{x})_i^2}$, where $\boldsymbol{D}_1$ and $\boldsymbol{D}_2$ respectively represent difference operators in the horizontal and vertical directions. $\mathrm{TV}(\boldsymbol{x})$ indicates the sparsity regularization of $\boldsymbol{x}$ in gradient domain, and it can be used to preserve edges of the images. $\eta > 0$ is a penalty parameter. The set C designates the data fidelity relation for the amplitudes and phases, which is employed to guarantee the image reconstruction accuracy from highly undersampled K-space data. The term $|\,|\boldsymbol{y}| - |\boldsymbol{F}_u\boldsymbol{x}|\,| \le \varepsilon$ is the amplitude errors between MR image measurements and undersampled K-space data of the reconstructed image (ε is the amplitude noise error). If there is no noise, ε is equal to 0, namely $|\boldsymbol{y}| = |\boldsymbol{F}_u\boldsymbol{x}|$. If the image measurements have noises, ε lies in the span $[2\sigma, 3\sigma]$ (σ is the Gaussian noise standard deviation). The term $|\angle\boldsymbol{y} - \angle\boldsymbol{F}_u\boldsymbol{x}| \le \delta$ represents the phase errors between measurements and undersampled K-space data of the reconstructed MR image ("$\angle$" represents the phase, and δ represents the phase error). If there is no phase error, δ equals 0, then the phase does not change, namely $\angle\boldsymbol{y} = \angle\boldsymbol{F}_u\boldsymbol{x}$. If the image measurements have motion artifacts, the two phases meet $|\angle\boldsymbol{y} - \angle\boldsymbol{F}_u\boldsymbol{x}| \le \delta$. Eq. (9) is sparse representation for MR images by exploiting sparse knowledge with LATF and TV in order to ensure the image reconstruction error minimum, and achieve better performances of the image reconstruction.

B. THE PROPOSED ALGORITHM
An alternating iterative minimization algorithm is developed to deal with the proposed model. The alternating minimization involves a learning $\boldsymbol{W}$ step and a solving $\boldsymbol{x}$ step.

1) ADAPTIVE TIGHT FRAME LEARNING

In the learning W step, we deal with the following problem with fixed x in Eq. (9):

$$\min_{W} \|Wx\|_{\log} \quad s.t. \; W^T W = I. \tag{10}$$

For the *n*th iteration, optimizing Eq. (10) with fixed x^{n-1} is implemented by the half-quadratic splitting algorithm. With introduction of a variable v, and assume $v = Wx$, we get the constrained version of Eq. (10) as

$$\{v^n, W^n\} = \underset{v,W}{\mathrm{argmin}}\{\left\|v - Wx^{n-1}\right\|_2^2 + \tau \|v\|_{\log}\}$$
$$s.t. \; W^T W = I. \tag{11}$$

In order to attack Eq. (11), Eq. (11) is divided into two sub-problems. The first sub-problem is to solve sparse coefficient v^n with fixed W^{n-1} as

$$v^n = \underset{v}{\mathrm{argmin}}\{\left\|v - W^{n-1}x^{n-1}\right\|_2^2 + \tau \|v\|_{\log}\}, \tag{12}$$

where $\tau > 0$ is a penalty parameter. Eq. (12) is a logarithm norm convex optimization problem, and the closed-form solution can be obtained exactly. The derivative of Eq. (12) can be simplified as the following equation:

$$v^3 - (W^{n-1}x^{n-1})v^2 + (1+\tau)v - (W^{n-1}x^{n-1}) = 0. \tag{13}$$

Here, the operator for v is element-wise. Eq. (13) can be solved in the form of the cubic equation root, that is Cardano formula (or use the method in [29]). However, the drawback of solving the cubic equation is that it takes more time. Therefore, one can borrow the LUT approach [30] to update v.

The second sub-problem is to update W^n according to v^n obtained by Eq. (12), and the expression is acquired as

$$W^n = \underset{W}{\mathrm{argmin}} \left\|v^n - Wx^{n-1}\right\|_2^2 \quad s.t. \; W^T W = I. \tag{14}$$

We employ the same method as Eq. (6) for this sub-problem. That is, we utilize SVD to derive the corresponding filters $\{a_i\}$ [26].

2) MR IMAGE RECONSTRUCTION

In the solving x step, Eq. (9) is solved with fixed W as

$$\min_{x} \|Wx\|_{\log} + \eta \mathrm{TV}(x) \quad s.t. \; x \in \mathrm{C}. \tag{15}$$

For the *n*th iteration, minimizing Eq.(15) with fixed W^n can be achieved. In this step, we solve Eq. (15) by the following problem

$$x^n = \arg\min_{x}\{\left\|W^n x\right\|_{\log} + \eta \mathrm{TV}(x)\} \quad s.t. \; x \in \mathrm{C}. \tag{16}$$

In this paper, we exploit the iPiano algorithm [31] to solve the Eq. (16).

In the process of attacking Eq. (16), we first let $f(x) = \left\|W^n x\right\|_{\log} + \eta \mathrm{TV}(x)$, and obtain its derivative
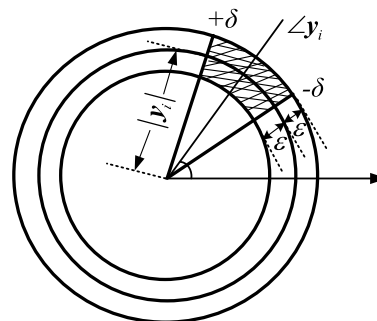
FIGURE 1. Shaded area is projection area of C.

$\nabla f(x) = \frac{2(W^n)^T}{1+(W^n x)^2} + \eta \frac{\partial \mathrm{TV}(x)}{\partial x}$. Then, we can formulate the following Eq.(17) by employing the iPiano algorithm:

$$x^{n-1/2} = x^{n-1} - \gamma \nabla f(x^{n-1}) + \beta(x^{n-1} - x^{n-2}). \tag{17}$$

Where, γ and β are the step size parameters. Project the intermediate variable $x^{n-1/2}$ onto the set C, and acquire the projection expression as following:

$$x^n = P_C(x^{n-1/2}) = F^{-1}(\left|G^n\right|e^{j\theta^n}). \tag{18}$$

Here, $P_C(\cdot)$ represents the projection operator, and $F^{-1}(\cdot)$ denotes the inverse Fourier transform operator. $\left|G^n\right|$ and θ^n indicate the projection magnitude and projection phase of $x^{n-1/2}$ respectively when $x^{n-1/2}$ is projected onto C. The set C expressed in polar coordinates is shown in Fig.1, where $\left|y_i\right|$ and $\angle y_i$ are the amplitude and phase of the *i*th measurement respectively. In Fig.1, the shaded area is the projection area of C, which is the possible area for projecting the *i*th value of $x^{n-1/2}$ onto it.

The expression of $\left|G_i^n\right|$ in Eq. (18) is described as following:

$$\left|G_i^n\right| = \begin{cases} \left|F_u x_i^{n-1/2}\right|, & \left|\left|F_u x_i^{n-1/2}\right| - \left|y_i\right|\right| \leq \varepsilon \\ \left|y_i\right| + \varepsilon, & \left|F_u x_i^{n-1/2}\right| - \left|y_i\right| > \varepsilon \\ \left|y_i\right| - \varepsilon, & \left|F_u x_i^{n-1/2}\right| - \left|y_i\right| < -\varepsilon. \end{cases} \tag{19}$$

Eq. (19) is the magnitude projection for the undersampled K-space measurement of the MR image. We do not consider the K-space data that are not taken sample because only the undersampled K-space data are updated in our algorithm. Similar to Eq. (19), Eq. (20) describes the phase projection for the undersampled measurement in K-space

$$\theta_i^n = \begin{cases} \angle F_u x_i^{n-1/2}, & \left|\angle F_u x_i^{n-1/2} - \angle y_i\right| \leq \delta \\ \angle y_i + \delta, & \angle F_u x_i^{n-1/2} - \angle y_i > \delta \\ \angle y_i - \delta, & \angle F_u x_i^{n-1/2} - \angle y_i < -\delta. \end{cases} \tag{20}$$

The implementing process of the TFTV-MRI model is as follows: first, we can obtain a general tight frame W_0 by learning lots of MR images, and generate an initial MR image x_0 by solving $F_u^H y$. Second, with fixed x_0, the adaptive tight frame W is updated n times. Then, with fixed W^n,
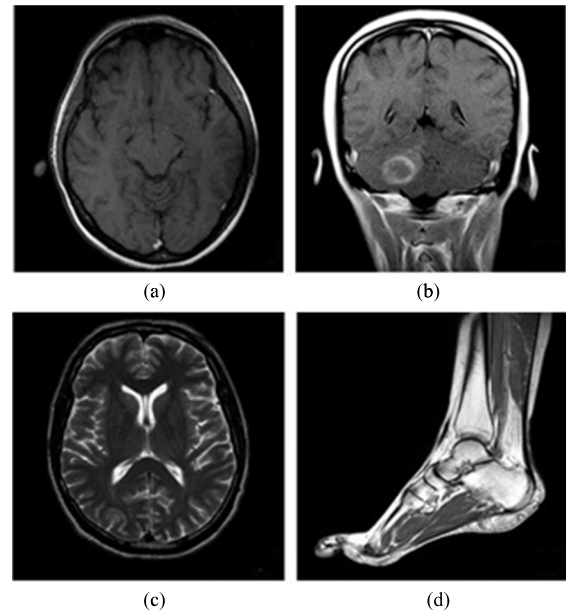
TABLE 1. The entire solving process of TFTV-MRI model.

Input：K-space measurement y; parameters η, γ, β; phase error δ; noise standard deviation σ; W iteration J_1; x iteration J_2; algorithm iteration J_3.
Output：Reconstructed MR image x.
(1) Initialization：$x^0 = F_u^H y$, $x^{-1} = 0$, W^0, τ^0, $k=0$.
(2) **while** $k < J_3$ **do**
(3)   **for** $n =1$ to J_1 **do**
(4)   Fixed x^k and W^{n-1}, update v^n according Eq. (12);
(5)   Fixed x^k and v^n, update W^n according Eq. (14);
(6)   **end for**
(7) $W^{k+1} \leftarrow W^n$
(8)   **for** $m =1$ to J_2 **do**
(9)   Fixed W^{k+1}, update x^m according Eq.(17)-(20);
(10)   **end for**
(11) $x^{k+1} \leftarrow x^m$
(12) $\tau^{k+1} = 1.1\tau^k$
(13) $k \leftarrow k+1$
(14) **end while**

FIGURE 2. MR test images. (a) BMR2; (b) Brain; (c) t2axialbrain; (d) foot-012.

the MR image is updated m times by using iPiano method. Third, the adaptive tight frame W^n is updated n times again by the updated image x^m. With fixed W^{2n}, and the MR image x^m is updated m times again by using iPiano method. Then, W^{2n} is updated n times by the updated image x^{2m}, ..., the above updating process is repeated until the stop criterion is met. The entire process for solving the proposed TFTV-MRI model is summarized in Table 1 as described.

IV. EXPERIMENTS AND DISCUSSION

A. EXPERIMENTAL SETUP

In order to verify the effectiveness of TFTV-MRI for reconstructing the image with phase noise or phase and amplitude noises, four standard test MR images with the same size of 512×512 are employed as the experimental images in this paper, as shown in Fig. 2. The experimental images are available in *http://www3.americanradiology.com/pls/web1/wwimggal.vmg*. In our experiments, the algorithm of TFTV-MRI was executed with 50 iterations to appraise its performance. We selected with the MR image block size of 9×9 and maximum patch overlap $r = 1$. We worked with $m = 1$ iterations to update the MR image. We selected with W block size of 81×81. We employed 12800 patches for LATF W learning, which was executed for 30 iterations. Zero-mean Gaussian noise of the standard deviation σ for the amplitude and random uniform distribution noise δ for the phase were added in MR image K-space respectively, and the amplitude noise error ε was selected as 3σ. The quality of the MR image reconstruction was evaluated by employing two metrics, PSNR and HFEN [19].

HFEN is utilized to describe the quality of MR image reconstruction of fine features and edges. The smaller the HFEN is, the better the edges and fine features of images are.

In order to check the image reconstruction performance of TFTV-MRI under different sampling schemes, 2D variable density random sampling (sampling rate R equals 12.5%) and pseudo radial sampling (the number of sampling line l equals 110) were performed on images to do reconstruction experiments. When reconstructing the MR image, along with phase noises produced by the translational motion of the patient, there is additive noise of the image amplitude in practical applications. Therefore, the simulation experiments in this paper included two parts: the ideal case with phase noise only, and the practical application case with phase and amplitude noises. The PSNR values of these two part experiment results were compared with those of Zero-filled, TLMRI, and TF-MRI, respectively. The TLMRI proposed in [14] is a blind CS MR image reconstruction model based on adaptive sparsifying transform learning. TLMRI is a better reconstruction model of CS kingdom in recent years. The TF-MRI model which only employs LATF learning is applied to MR image reconstruction with phase and amplitude noises. TF-MRI based on making use of the sparse priors of the MR image via ATF learning. That is to say, the TF-MRI that is proposed in this paper is special form of Eq. (8) where the penalty parameter η is equal to 0. The TF-MRI model is sparse representation for MR images by exploiting sparse knowledge with LATF only, excluding TV regularization.

B. EXPERIMENTAL RESULTS AND DISCUSSION

In order to verify the image reconstruction quality and anti-noise performance of TFTV-MRI with the phase noise only,

TABLE 2. Comparisons of MR image reconstruction PSNR values (dB) with phase noises only.

Images	Models	2D random sampling (R=12.5%)				Pseudo radial sampling (l=110)			
		$\delta=\pi/24$	$\delta=\pi/18$	$\delta=\pi/12$	Average	$\delta=\pi/24$	$\delta=\pi/18$	$\delta=\pi/12$	Average
BMR2	Zero-filled	24.41	25.15	24.47	24.68	29.62	28.96	27.47	28.68
	TLMRI	35.19	33.02	29.75	32.65	34.26	33.33	32.34	33.31
	TF-MRI	38.39	37.32	35.73	37.15	35.23	34.89	34.18	34.78
	TFTV-MR	**39.84**	**38.74**	**37.12**	**38.57**	**38.86**	**38.29**	**37.07**	**38.07**
Brain	Zero-filled	20.35	20.09	19.44	19.96	26.32	25.36	23.41	25.03
	TLMRI	30.47	28.15	24.78	27.80	30.49	28.51	26.39	28.46
	TF-MRI	34.90	33.69	31.89	33.49	33.52	32.97	32.04	32.84
	TFTV-MR	**37.36**	**36.24**	**33.36**	**35.65**	**35.82**	**35.06**	**33.46**	**34.78**
t2axialbrain	Zero-filled	24.77	24.51	24.01	24.43	28.82	28.28	27.05	28.05
	TLMRI	35.56	33.41	30.16	33.04	34.36	32.80	31.15	32.77
	TF-MRI	39.99	38.97	37.37	38.78	34.48	34.11	33.53	34.04
	TFTV-MR	**41.45**	**40.71**	**39.16**	**40.44**	**38.08**	**37.63**	**36.63**	**37.45**
foot-012	Zero-filled	20.04	19.76	19.06	19.62	24.96	24.11	22.34	23.80
	TLMRI	29.90	27.66	24.34	27.30	29.17	27.41	25.51	27.36
	TF-MRI	36.98	36.30	35.10	36.12	31.45	31.14	30.80	31.13
	TFTV-MR	**38.65**	**38.17**	**37.19**	**38.00**	**34.29**	**34.14**	**33.75**	**34.06**

the experiments were carried out for MR test images. In this case, the amplitude noise error $\varepsilon = 0$, and the phase error δ is respectively selected as $\pi/24$, $\pi/18$ and $\pi/12$ in the set C of Eq. (8). A large number of experiments affirm that the better image reconstruction results can be achieved when the values of various parameters are set as $\tau^0 = 0.5$, $\eta = 0.8$, $\gamma = 0.001$, $\beta = 0.002$ in TFTV-MRI, $\tau = 0.7$, $\gamma = 0.001$ in TF-MRI and $s = 0.065$ (Other parameters are the same as in [14]) in TLMRI for 2D variable density random sampling; meanwhile $\tau^0 = 0.5$, $\eta = 1.5$, $\gamma = 0.001$, $\beta = 0.015$ in TFTV-MRI, $\tau = 0.6$, $\gamma = 0.001$ in TF-MRI and $s = 0.035$ (Other parameters are the same as in [14]) in TLMRI for pseudo radial sampling. The experimental results of three different phase noises in TFTV-MRI are compared with the each contrast model respectively, as shown in Table 2. From the data in Table 2, it can be observed that the average PSNR values of the reconstructed each image by using TFTV-MRI are larger than each of the contrast models. In Table 2, the BMR2 image is taken as an example. The average PSNR values of the reconstructed image using TFTV-MRI increase by 1.42dB and 5.92dB respectively compared with TF-MRI and TLMRI under three different phase noises by employing 2D variable density random sampling, and increase by 3.29dB and 4.76dB respectively compared with TF-MRI and TLMRI in three different phase noises by employing pseudo radial sampling. Hence, TFTV-MRI can achieve the better reconstruction quality of the MR image, and can effectively remove the phase noises of motion artifacts. The proposed model can perform reconstruction effectiveness, better anti-noise and robustness performance to achieve phase denoising of MR images.

In order to investigate the image reconstruction quality and anti-noise performance of TFTV-MRI with the phase noise and amplitude noise simultaneous, the experiments were executed. In this case, the phase error $\delta = \pi/24$, the noise standard deviation σ is respectively selected as 15, 20 and 25, and the amplitude noise error $\varepsilon = 3\sigma$ in the set C of Eq. (8). The experimental results of TFTV-MRI with different amplitude noises and the unique phase noise were compared with the each contrast model respectively, as shown in Table 3. From Table 3, we can see that the average PSNR value of the reconstructed each image by employing TFTV-MRI is superior to the each contrast model in the two sampling schemes when the amplitude noise and phase noise are included. In Table 3, Brain image is taken as an example. The average PSNR values of the reconstructed image of TFTV-MRI increase by 1.75dB and 5.20dB respectively compared with TF-MRI and TLMRI under three different amplitude noise deviations by employing 2D variable density random sampling, and increase by 1.33dB and 3.85dB respectively compared with TF-MRI and TLMRI by employing pseudo radial sampling. TFTV-MRI can also improve the quality of the MR image reconstruction, and can effectively remove the phase and amplitude noises simultaneously, with better anti-noise and robustness performances.

In order to illustrate the convergence and superiority properties of TFTV-MRI, Fig.3 shows the PSNR curves of the reconstructed BMR2 image changing with the iteration number. In Fig.3, the PSNR curve of TFTV-MRI compares with the three contrast models in 2D variable density random sampling scheme (the amplitude noise standard deviation $\sigma = 20$, and the phase error $\delta = \pi/24$). With the same

TABLE 3. Comparisons of MR image reconstruction PSNR values (dB) with amplitude and phase noises.

| Images | Models | 2D random sampling (R=12.5%) Phase noise (δ=π/24) | | | | Pseudo radial sampling (l=110) Phase noise (δ=π/24) | | | |
		σ=15	σ=20	σ=25	Average	σ=15	σ=20	σ=25	Average
BMR2	Zero-filled	25.36	25.31	25.26	25.31	29.38	29.20	28.99	29.19
	TLMRI	34.53	34.07	33.54	34.05	34.02	33.44	32.68	33.38
	TF-MRI	36.52	35.72	34.78	35.67	34.48	33.89	33.33	33.90
	TFTV-MRI	**38.20**	**37.05**	**35.82**	**37.02**	**36.88**	**35.82**	**34.71**	**35.80**
Brain	Zero-filled	20.33	20.32	20.30	20.32	26.21	26.12	26.01	26.11
	TLMRI	30.25	30.08	29.87	30.07	30.23	30.04	29.80	30.02
	TF-MRI	34.09	33.55	32.91	33.52	33.03	32.52	32.06	32.54
	TFTV-MRI	**36.21**	**35.33**	**34.27**	**35.27**	**34.62**	**33.91**	**33.09**	**33.87**
t2axialbrain	Zero-filled	24.71	24.67	24.62	24.67	28.61	28.45	28.26	28.44
	TLMRI	34.82	34.32	33.75	34.30	33.69	33.22	32.71	33.21
	TF-MRI	37.08	36.00	35.11	36.06	33.99	33.44	32.58	33.34
	TFTV-MRI	**38.14**	**37.01**	**35.86**	**37.00**	**35.93**	**34.95**	**33.89**	**34.92**
foot-012	Zero-filled	20.02	20.00	19.98	20.00	24.87	24.80	24.71	24.79
	TLMRI	29.67	29.49	29.27	29.48	28.93	28.76	28.55	28.75
	TF-MRI	34.84	34.20	33.13	34.06	31.14	30.74	30.31	30.73
	TFTV-MRI	**35.91**	**35.08**	**34.15**	**35.38**	**32.97**	**32.22**	**31.57**	**32.25**
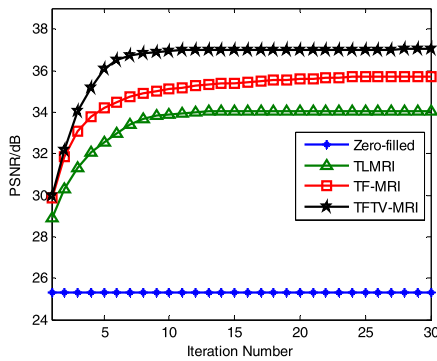
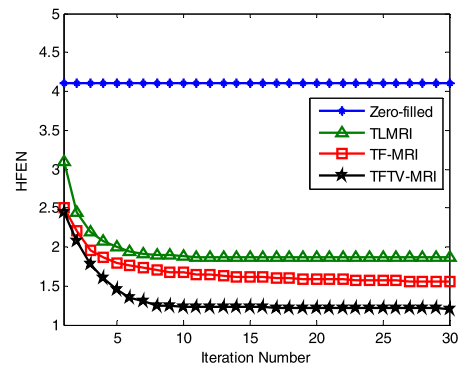**FIGURE 3.** PSNR curves of BMR2 image along with iterations.

FIGURE 4. HFEN curves of BMR2 image along with iterations.

condition as in Fig.3, Fig.4 displays the HFEN curves of the four models changing with the iteration number. It can be seen from Fig.3 that the convergence speed of TFTV-MRI is fastest. TFTV-MRI has a faster convergence speed and the larger PSNR value, which is obviously superior to TF-MRI and TLMRI. Fig.4 exhibits that TFTV-MRI has the smaller HFEN value which reveals the better edge structure of the reconstructed image, compared to those of TF-MRI and TLMRI.

However, PSNR and HFEN cannot represent perceptual visual quality, which can only be accurately evaluated by human visual observer studies [19]. In order to further demonstrate the superiority of TFTV-MRI, image reconstruction qualities were evaluated from visual inspection. For a visual comparison, Fig.5 and Fig.6 illustrate the reconstructed results of the image ''Brain'' with the phase noise ($\delta = \pi/24$) and the amplitude noise ($\sigma = 20$) via 2D variable density

random sampling. Fig.6 exhibits reconstructed results of the magnified region for the Brain image. As can be seen from Fig.5, there are serious partial losses in the reconstructed image details by using TLMRI and TF-MRI. While TFTV-MRI can better reconstruct the original image, there are more details in the reconstructed image such as the textures and contours with respect to the brain. It also can be seen from Fig.6 that compared with the three contrast models, TFTV-MRI has been obviously improved the quality of the reconstructed image, preserved more image details, and better removed phase and amplitude noises. For a close-up comparison in Fig.6, we enlarged the part of Brain image, from which we can judge that TFTV-MRI provides clearer details.

In conclusion, the quality of the reconstructed MR image by employing Zero-filled is the worst of the four models. Reconstructed MR images lost lots of detail information, and
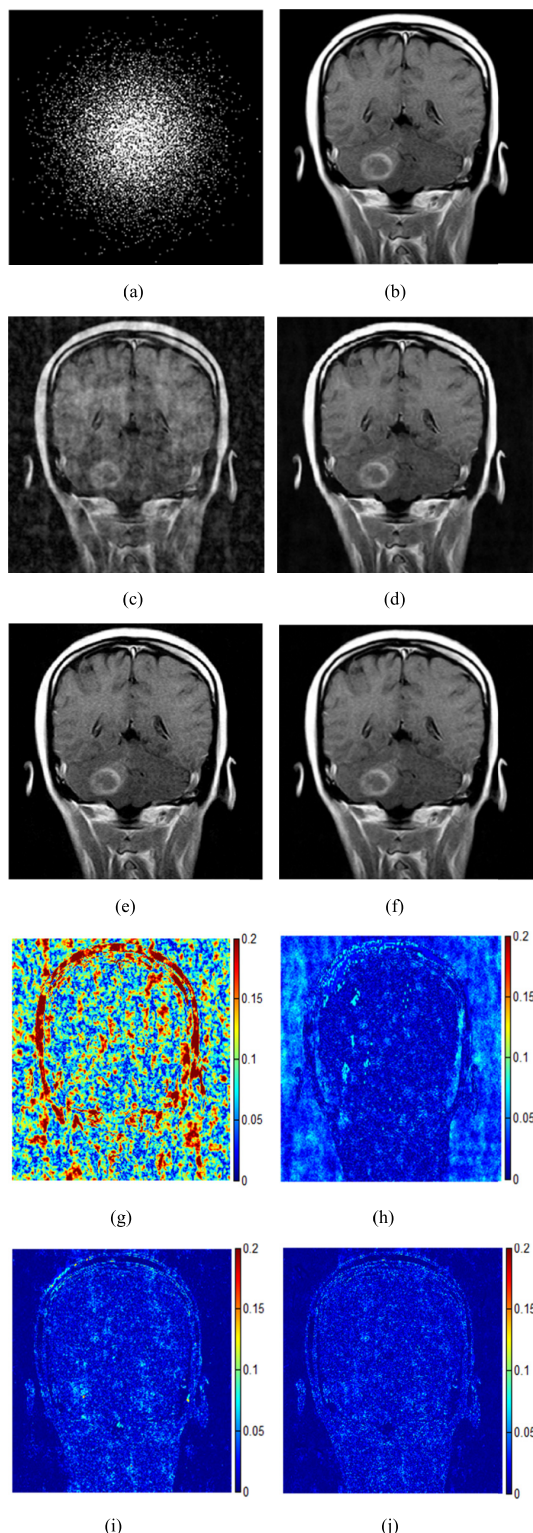
(a)　　　　　　　　(b)

(c)　　　　　　　　(d)

(e)　　　　　　　　(f)

(g)　　　　　　　　(h)

(i)　　　　　　　　(j)

FIGURE 5. Reconstruction results and error magnitudes of Brain image with 2D variable density random sampling (a) Sampling in the K-space; (b) Original image; (c), (d), (e) and (f) are reconstruction results for Zero-filled, TLMRI, TF-MRI and TFTV-MRI; (g), (h), (i) and (j) are reconstruction error magnitudes for Zero-filled, TLMRI, TF-MRI and TFTV-MRI, respectively.

blur the parts of smoothness and edges. The quality of the reconstructed image by using TLMRI is better than that of Zero-filled, but it still loses some detail information caused by
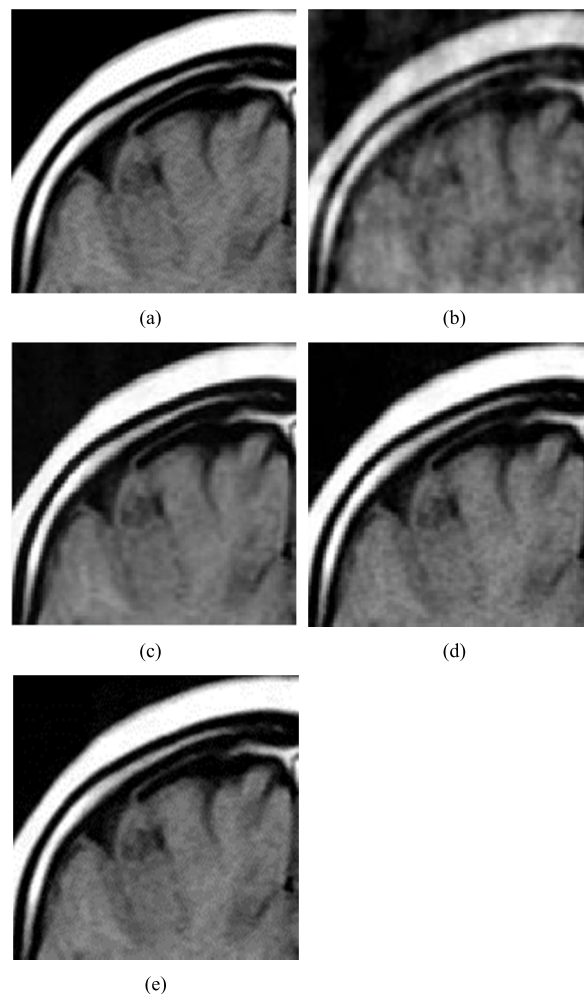

(a)　　　　　　　　(b)

(c)　　　　　　　　(d)

(e)

FIGURE 6. Reconstruction results of the local Brain image (a) Original image; (b) Zero-filled; (c) TLMRI; (d) TF-MRI; (e) TFTV-MRI.

excessive smoothness of the image and fuzziness of the edge contour structure. The image reconstruction quality of the TF-MRI is better than that of TLMRI, but it still loses some detail information with further clearness of edge contour structure. TFTV-MRI can more accurately reconstruct detail information and edge contour structure, and can remove the phase and amplitude noises.

The above experimental results demonstrate that the MR image reconstruction of TFTV-MRI improves remarkably compared with TF-MRI and TLMRI. This is because that TFTV-MRI exploits the sparse prior knowledge of the MR image in virtue of LATF learning and TV regularization, TF-MRI exploits the sparse prior knowledge of the image in virtue of LATF learning only, and TLMRI exploits the sparse prior knowledge under the adaptive sparsity-ing transform learning only. In TFTV-MRI, LATF learning is applied to the image reconstruction model. Then, according to the cooperation between the LAFT regularization and TV regularization, the quality of the reconstructed MR image is further improved. Moreover, more detail and edge contour structure information is obtained.

Hence, TFTV-MRI becomes more effective and more applicable.

V. CONCLUSIONS

A novel TFTV-MRI model has been proposed to effectively reconstruct MR image from highly undersampled K-space data in this paper. This model combines LATF learning with TV regularization which can preserve edges of the MR image. The two kinds of sparse priors are applied to the TFTV-MRI model simultaneously, whose advantage is that it exploits the sparse prior knowledge both in the frame domain and in the gradient domain. Furthermore, we employ the alternating iterative minimization algorithm to solve the TFTV-MRI effectively, in which we bring the LUT algorithm, SVD and the iPiano algorithm. Various experiment results demonstrate that the proposed TFTV-MRI achieves the superior performance for MR image reconstruction in artifacts suppression, detail clarity, and edge preservation with both phase noises and amplitude noises. The proposed model also illustrates highly accurate MR image reconstruction over the other two models including TF-MRI and TLMRI, due to the TFTV-MRI utilizes many advantages, for example, the MR image and its gradient can be represented much sparser by using LATF learning and TV regularization respectively. TFTV-MRI has better robustness, and faster convergence speed than those of TF-MRI and TLMRI. TFTV-MRI will contribute to the clinical application of MR images. How to exploit more sparse priors for the MR image reconstruction, how to further improve the image reconstruction performance, and how to farther implement fast and accurately image reconstruction with lower sampling rate are all the future research aspects.

REFERENCES

[1] P. Padilla, J. F. Valenzuela-Valdés, J. L. Padilla, and F. Luna-Valero, "Electromagnetic near-field inhomogeneity reduction for image acquisition optimization in high-resolution multi-channel magnetic resonance imaging (MRI) systems," *IEEE Access*, vol. 5, pp. 5149–5157, 2017, doi: 10.1109/ACCESS.2017.2685079.

[2] M. Hedley, H. Yan, and D. Rosenfeld, "Motion artifact correction in MRI using generalized projections," *IEEE Trans. Med. Imag.*, vol. 10, no. 1, pp. 40–46, Mar. 1991.

[3] R. A. Zoroofi, Y. Sato, S. Tamura, H. Naito, and L. Tang, "An improved method for MRI artifact correction due to translational motion in the imaging plane," *IEEE Trans. Med. Imag.*, vol. 14, no. 3, pp. 471–479, Sep. 1995.

[4] S. Marchesini, "Invited article: A unified evaluation of iterative projection algorithms for phase retrieval," *Rev. Sci. Instrum.*, vol. 78, no. 1, p. 011301, 2007.

[5] Y. M. Kadah, A. A. Abaza, A. S. Fahmy, A. B. Youssef, K. Heberlein, and X. P. Hu, "Floating navigator echo (FNAV) for in-plane 2D translational motion estimation," *Magn. Reson. Med.*, vol. 51, no. 2, pp. 403–407, 2004.

[6] W. Lin, F. Huang, P. Börnert, Y. Li, and A. Reykowski, "Motion correction using an enhanced floating navigator and GRAPPA operations," *Magn. Reson. Med.*, vol. 63, no. 2, pp. 339–348, 2010.

[7] C.-X. Chen, H. Tao, and S. J. Wang, "Motion artifact correction in MRI using genetic algorithms," *J. Image Graph.*, vol. 10, no. 9, pp. 1129–1133, 2005.

[8] J. Mendes, E. Kholmovski, and D. L. Parker, "Rigid-body motion correction with self-navigation MRI," *Magn. Reson. Med.*, vol. 61, no. 3, pp. 739–747, 2009.

[9] J. Ma, J. B. Son, and J. D. Hazle, "An improved region growing algorithm for phase correction in MRI," *Magn. Reson. Med.*, vol. 76, no. 2, pp. 519–529, 2016.

[10] D. L. Donoho, "Compressed sensing," *IEEE Trans. Inf. Theory*, vol. 52, no. 4, pp. 1289–1306, Apr. 2006.

[11] E. J. Candes, J. Romberg, and T. Tao, "Robust uncertainty principles: Exact signal reconstruction from highly incomplete frequency information," *IEEE Trans. Inf. Theory*, vol. 52, no. 2, pp. 489–509, Feb. 2006.

[12] Y. Zhang, J. Yang, J. Yang, A. Liu, and P. Sun, "A novel compressed sensing method for magnetic resonance imaging: Exponential wavelet iterative shrinkage-thresholding algorithm with random shift," *Int. J. Biomed. Imag.*, vol. 2016, no. 3, 2016, Art. no. 9416435.

[13] Z. Y. Li, G. Li, Y. Sun, G. Chen, and S. H. Luo, "A denoising method for low-dose small-animal computed tomography image based on globe dictionary learning," *J. Biomed. Eng.*, vol. 33, no. 2, pp. 279–286, Apr. 2016.

[14] S. Ravishankar and Y. Bresler, "Efficient blind compressed sensing using sparsifying transforms with convergence guarantees and application to magnetic resonance imaging," *SIAM J. Imag. Sci.*, vol. 8, no. 4, pp. 2519–2557, 2015.

[15] Y. Liu *et al.*, "Balanced sparse model for tight frames in compressed sensing magnetic resonance imaging," *PLoS ONE*, vol. 10, no. 4, p. e0119584, 2015.

[16] J. Huang, L. Guo, Q. Feng, W. Chen, and Y. Feng, "Sparsity-promoting orthogonal dictionary updating for image reconstruction from highly undersampled magnetic resonance data," *Phys. Med. Biol.*, vol. 60, no. 14, pp. 5359–5380, 2015.

[17] M. Lustig, D. Donoho, and J. M. Pauly, "Sparse MRI: The application of compressed sensing for rapid MR imaging," *Magn. Reson. Med.*, vol. 58, no. 6, pp. 1182–1195, 2007.

[18] J. K. Barral and D. G. Nishimura, "Compressed sensing for motion artifact reduction," in *Proc. Int. Soc. Magn. Reson. Med.*, 2009, p. 4593.

[19] S. Ravishankar and Y. Bresler, "MR image reconstruction from highly undersampled k-space data by dictionary learning," *IEEE Trans. Med. Imag.*, vol. 30, no. 5, pp. 1028–1041, May 2011.

[20] S. Ravishankar and Y. Bresler, "Sparsifying transform learning for compressed sensing MRI," in *Proc. IEEE Int. Symp. Biomed. Imag.*, Apr. 2013, pp. 17–20.

[21] Z. Yang, C. Zhang, and L. Xie, "Sparse MRI for motion correction," in *Proc. IEEE 10th Int. Symp. Biomed. Imag.*, Apr. 2013, pp. 962–965.

[22] J. Liu, S. Wang, X. Peng, and D. Liang, "Undersampled MR image reconstruction with data-driven tight frame," *Comput. Math. Methods Med.*, vol. 2015, no. 1, Jun. 2015, Art. no. 424087.

[23] F. Dong, Q. F. Wang, H. Zheng, Z. M. Li, G. Yang, and J. Q. Li, "Motion artifacts correction in MRI with navigator echo combined with compressed sensing," *Chinese J. Magn. Reson.*, vol. 32, no. 3, pp. 419–428, Sep. 2015.

[24] J. Yang, Y. Zhang, and W. Yin, "A fast alternating direction method for TVL1-L2 signal reconstruction from partial Fourier data," *IEEE J. Sel. Topics Signal Process.*, vol. 4, no. 2, pp. 288–297, Apr. 2010.

[25] Q. G. Liu, S. Wang, L. Ying, X. Peng, Y. Zhu, and D. Liang, "Adaptive dictionary learning in sparse gradient domain for image recovery," *IEEE Trans. Image Process.*, vol. 22, no. 12, pp. 4652–4663, Dec. 2013.

[26] J.-F. Cai, H. Ji, Z. Shen, and G.-B. Ye, "Data-driven tight frame construction and image denoising," *Appl. Comput. Harmon. Anal.*, vol. 37, no. 1, pp. 89–105, 2014.

[27] Z. Zhan, J.-F. Cai, D. Guo, Y. Liu, Z. Chen, and X. Qu, "Fast multiclass dictionaries learning with geometrical directions in MRI reconstruction," *IEEE Trans. Biomed. Eng.*, vol. 63, no. 9, pp. 1850–1861, Sep. 2015.

[28] Y. Deng, Q. Dai, R. Liu, Z. Zhang, and S. Hu, "Low-rank structure learning via nonconvex heuristic recovery," *IEEE Trans. Neural Netw. Learn. Syst.*, vol. 24, no. 3, pp. 383–396, Mar. 2013.

[29] E. W. Weisstein. (2017). "Cubic Formula." [Online]. Available: http://mathworld.wolfram.com/CubicFormula.html

[30] D. Krishnan and R. Fergus, "Fast image deconvolution using hyper-Laplacian priors," in *Proc. NIPS*, 2009, pp. 1033–1041.

[31] P. Ochs, Y. Chen, T. Brox, and T. Pock, "iPiano: Inertial proximal algorithm for nonconvex optimization," *SIAM J. Imag. Sci.*, vol. 7, no. 2, pp. 1388–1419, 2014.

FAN XIAOYU was born in 1981. He received the M.S. degree. He is currently pursuing the Ph.D. degree in electronic science and technology with Yanshan University. He joined as a Lecturer with the Anhui Science and Technology University. His research interests include signal and image processing, compressed sensing, sparse representation, and dictionary learning.

SHI BAOSHUN was born in 1989. He received the Ph.D. degree from Yanshan University. He is currently a Post-Doctoral Researcher with Yanshan University, China. His current research interests include signal and image processing, blind compressed sensing, sparse representation, dictionary learning, and phase retrieval.

• • •

LIAN QIUSHENG was born in 1969. He received the Ph.D. degree from Yanshan University. He is currently a Professor with the School of Information Science and Engineering, Yanshan University, China. His current research interests include signal and image processing, compressed sensing, sparse representation, phase retrieval, and deep learning.